

Nanoscale topography-capacitance correlation in high- K films: Interface heterogeneity related electrical properties

Cite as: J. Appl. Phys. **98**, 076104 (2005); <https://doi.org/10.1063/1.2077840>

Submitted: 11 May 2005 • Accepted: 29 August 2005 • Published Online: 06 October 2005

J. M. Sturm, A. I. Zinine, H. Wormeester, et al.



View Online



Export Citation

ARTICLES YOU MAY BE INTERESTED IN

[Edge effects in intermetallic compound crystal growth between Nb and molten 52In-48Sn solder](#)

Applied Physics Letters **88**, 104105 (2006); <https://doi.org/10.1063/1.2186392>

[Crack detection and analyses using resonance ultrasonic vibrations in full-size crystalline silicon wafers](#)

Applied Physics Letters **88**, 111907 (2006); <https://doi.org/10.1063/1.2186393>

[Nanodevice design through the functional abstraction of biological macromolecules](#)

Applied Physics Letters **87**, 143902 (2005); <https://doi.org/10.1063/1.2077839>



Time to get excited.
Lock-in Amplifiers – from DC to 8.5 GHz

Find out more

Zurich Instruments

Nanoscale topography-capacitance correlation in high-*K* films: Interface heterogeneity related electrical properties

J. M. Sturm,^{a)} A. I. Zinine, H. Wormeester, and Bene Poelsema

Solid State Physics Group, MESA+ Institute for Nanotechnology, University of Twente, P.O. Box 217, 7500 AE Enschede, The Netherlands

R. G. Bankras, J. Holleman, and J. Schmitz

Semiconductor Components Group, MESA+ Institute for Nanotechnology, University of Twente, P.O. Box 217, 7500 AE Enschede, The Netherlands

(Received 11 May 2005; accepted 29 August 2005; published online 6 October 2005)

Kelvin probe force microscopy in ultrahigh vacuum was used to study inhomogeneities of the contact potential difference (CPD) and differential capacitance of thin atomic layer deposited Al_2O_3 films. CPD fluctuations correlate equally strongly with the surface topography for deposition on hydrogen-terminated Si and thermal SiO_2 . The correlation of the differential capacitance with the topography clearly distinguishes films based on the starting surface. The lateral electrical homogeneity of these thin oxides depends crucially on their initial nucleation. © 2005 American Institute of Physics. [DOI: 10.1063/1.2077840]

The downscaling of the gate dielectric in complementary metal-oxide-semiconductor technology has led to a dramatic increase in gate leakage current. Further downscaling will soon require high-*K* gate dielectrics, such as metal oxides, as a replacement for the conventional SiO_2 .¹ Among possible deposition techniques, atomic layer deposition (ALD) has great potential because of its excellent thickness control and uniformity for large area deposition due to the self-limited nature of this deposition process. However, deposition of metal oxides on hydrogen-terminated Si usually suffers from a lack of reactive sites of the starting surface, resulting in a lower growth per cycle in the first cycles of deposition compared to the equilibrium growth rate that is achieved when the metal oxide fully covers the substrate.² This behavior, called substrate-inhibited ALD, leads to the formation of dispersed nuclei at the start of the ALD growth and can result in an inhomogeneous film thickness and poor film quality.³ Problems with substrate inhibition can be circumvented by growing a thermal or chemical SiO_2 layer before deposition of the high-*K* oxide.^{2,4} However, this lowers the total capacitance of the gate stack and therefore a high-quality metal oxide film directly on Si is preferred. Substrate inhibition has been extensively studied with measurements of the growth per cycle^{2,4} and the resulting nuclei have been resolved in transmission electron microscopy pictures.³ However, both methods cannot directly link the observed growth rate or morphology with electrical characteristics. Recent Kelvin probe force microscopy (KPFM) measurements showed that HfO_2 and SiO_2 crystallites in a phase-separated silicate film could be visualized in topography, contact potential difference (CPD), and tip-sample capacitance images.⁵ Recently we showed a correlation between CPD and topography for 2.5 nm atomic layer deposited Al_2O_3 films on hydrogen-terminated Si.⁶ Although this correlation might be partly related to the presence of nuclei in the film, it is probably

difficult to observe substrate inhibition from the CPD signal, since CPD fluctuations can also be caused by variations in the interface state density and doping concentration.⁵ In this communication we present CPD and differential capacitance measurements on thermal SiO_2 and ALD grown Al_2O_3 films, deposited directly on Si (with substrate inhibition) and on SiO_2 (noninhibited). By linking the spatial variation of the capacitance with the simultaneously acquired surface topography, thickness variations due to nucleation of the growth process can be revealed. This method provides a direct way to visualize substrate-inhibited ALD growth and proves to be successful in distinguishing the growth mode of the three types of samples studied.

Si (001) samples (boron doped, $N_A=10^{15} \text{ cm}^{-3}$) were cleaned in fuming and boiling nitric acid (HNO_3 100% and 69%, respectively), followed by a 1% HF dip in order to remove the native oxide layer. Subsequently, the samples were introduced in a home-built ALD reactor (base pressure $< 10^{-7}$ mbar), where Al_2O_3 was deposited from trimethylaluminum and water vapor at 300 °C. Alternatively, a 2.2 nm SiO_2 film was grown by thermal oxidation prior to deposition of the Al_2O_3 . In order to verify whether the deposition was substrate inhibited or not, the deposited amount of aluminum oxide after one to four cycles of deposition was determined by x-ray photoelectron spectroscopy (XPS). The growth rate on hydrogen-terminated (HF last) silicon was significantly reduced with respect to deposition on thermal SiO_2 . Deposition on thermal and chemical SiO_2 (grown in boiling nitric acid) shows an identical initial growth behavior. This indicates that the ALD process is substrate inhibited on hydrogen-terminated silicon, but not on thermal SiO_2 , in line with Ref. 2. After deposition, samples were loaded in a RHK UHV 450 beam-deflection AFM (base pressure $< 10^{-10}$ mbar) used in frequency modulated (FM) noncontact AFM mode with the aid of a Nanosurf EasyPLL FM demodulator. Electrostatic interactions were probed by FM Kelvin/CPD imaging⁷ and differential capaci-

^{a)}Electronic mail: j.m.sturm@utwente.nl

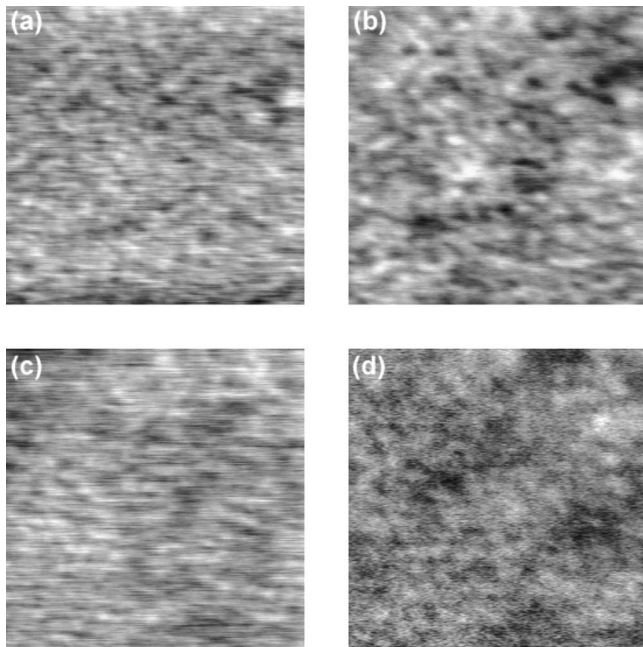


FIG. 1. $1 \times 1 \mu\text{m}^2$ topography (height scale 0.25 nm) (a) and CPD image (height scale 80 mV) (b) of a Si/2.2 nm SiO₂/1.0 nm Al₂O₃ sample; (c) and (d) represent topography (height scale 0.16 nm) and CPD (height scale 70 mV) for a 2.2 nm SiO₂ film without Al₂O₃ on top.

tance imaging,⁵ using cantilevers (nominal resonance frequency 75 kHz) with a conductive coating.⁸ The sample bias was modulated with a 1 kHz, 0.5 V rms sine wave and the electrostatic tip-sample interaction (Kelvin signal) was measured by feeding the demodulated output from the phase-locked loop detector in a lock-in amplifier tuned to the bias modulation frequency. For CPD images the Kelvin signal was fed into a feedback loop that adjusted the dc bias to nullify the Kelvin signal. Finally, differential capacitance measurements were performed by measuring the lock-in signal at the second harmonic of the bias modulation (CPD feedback disabled). This signal is proportional to $\partial^2 C / \partial z^2$ (with C the tip-sample capacitance and z the coordinate along the surface normal) and is independent of the CPD.⁵ CPD images were also constructed from tip height versus voltage spectra with active feedback⁶ in order to exclude modulation artifacts. Quantitative comparison of the similarity of a topographic and electrical (CPD or capacitance) image was obtained from their cross correlation. The cross correlation $c_{fg}(\mathbf{r})$ of two images $f(\mathbf{x})$ and $g(\mathbf{x})$ is mathematically represented by

$$c_{fg}(\mathbf{r}) = \int_{\mathbf{x}} f(\mathbf{x})g(\mathbf{x} + \mathbf{r})d\mathbf{x}, \quad (1)$$

where the integration runs over all values of the lateral coordinate vector \mathbf{x} . The similarity between image f and image g (shifted over a distance \mathbf{r} with respect to f) is represented by $c_{fg}(\mathbf{r})$. The cross correlation thus behaves as pattern recognition: peaks in the cross-correlation image indicate similarity of the images for the corresponding \mathbf{r} and the peak height is a quantitative measure for the similarity.⁹

Figure 1 shows topography and CPD images of a Si/SiO₂/1 nm Al₂O₃ and a Si/SiO₂ sample. Both images

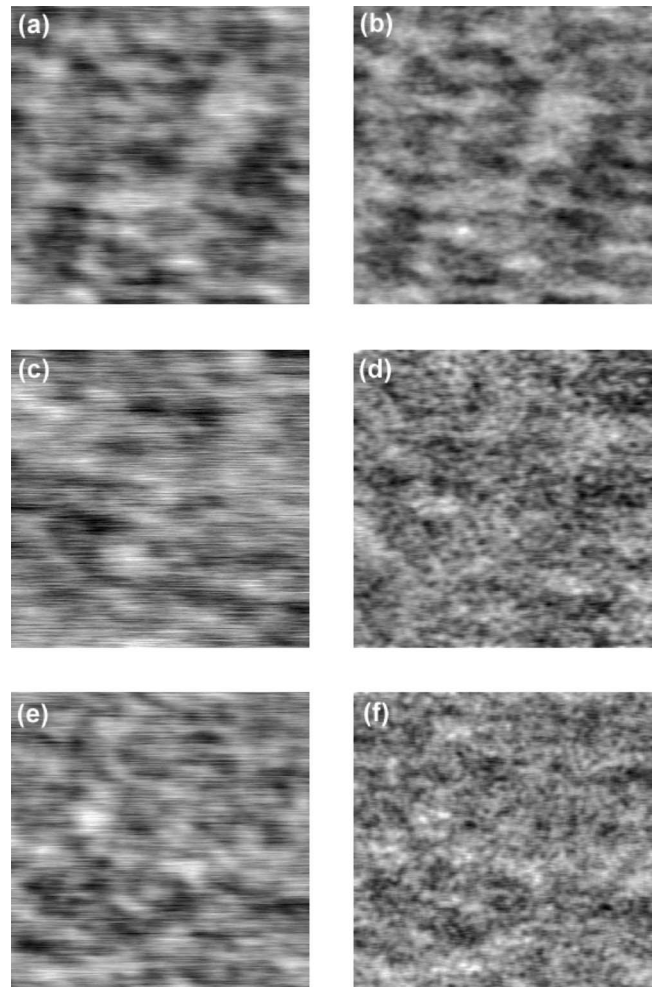


FIG. 2. $0.5 \times 0.5 \mu\text{m}^2$ topography (left images) and differential capacitance (right images) of 2.5 nm Al₂O₃ on HF last Si [(a), (b)], 2.2 nm thermal SiO₂ [(c), (d)], and 2.0 nm Al₂O₃ on 2.2 nm SiO₂ [(e), (f)]. The height scale of the capacitance images ranges from high capacitance (black) to low (white). The height scales of the topographic images are (a) 0.22 nm, (c) 0.20 nm, and (e) 0.22 nm.

show correlation between the topography and CPD signal for features with a lateral scale of 50–100 nm. Si/SiO₂/2 nm Al₂O₃ samples and Al₂O₃ directly deposited on HF stripped Si show a similar correlation. The differential capacitance image (Fig. 2) shows a very similar pattern to the topography for the Al₂O₃ film deposited on hydrogen-terminated silicon. A high topography signal correlates with a low capacitance and vice versa. Such a strong correlation cannot be seen by the eye for the thermal SiO₂ sample. The samples with 1 or 2 nm Al₂O₃ on thermal oxide show a lower amount of correlation with respect to Al₂O₃ on silicon. In order to quantify the correlation, the cross correlation between the topography and the simultaneously acquired CPD or differential capacitance image was calculated using a normalized height scale for all images. Figure 3(a) shows the intensity profiles through the center line of the topography-differential capacitance cross-correlation images for all four investigated samples. The height of the peak indicates the degree of correlation between topography and capacitance and the width the typical lateral size on which the correlation occurs. The analysis was carried out on $1 \times 1 \mu\text{m}^2$ and 0.5

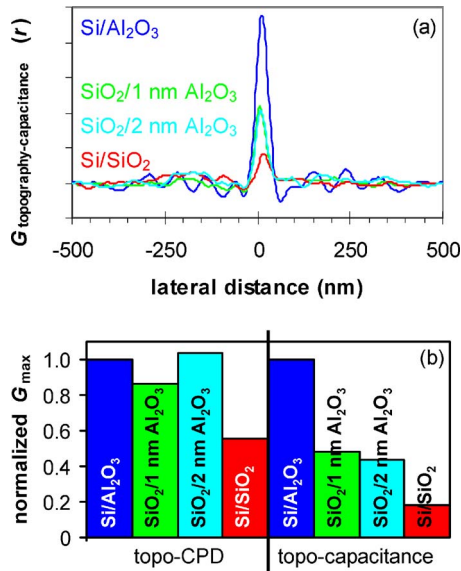


FIG. 3. (Color online) (a) Cross correlation $G(r)$ of $1 \times 1 \mu\text{m}^2$ topography and differential capacitance images of 2.5 nm Al_2O_3 on HF last Si (blue), 2.2 nm thermal SiO_2 (red), 1.0 nm Al_2O_3 on 2.2 nm SiO_2 (green), and 2.0 nm Al_2O_3 on 2.2 nm SiO_2 (cyan). (b) Maximum of cross-correlation peak G_{max} of topography with CPD and topography with differential capacitance. Values are relative to the G_{max} value for Al_2O_3 on HF last Si.

$\times 0.5 \mu\text{m}^2$ images and in both cases the degree of correlation and typical lateral size were identical. Figure 3(b) summarizes the results obtained with the cross-correlation procedure for both CPD and capacitance measurements. The values in this plot are normalized with respect to the maximum of the cross correlation for Al_2O_3 deposited on hydrogen-terminated silicon.

The measurement of the CPD fluctuations on the $\text{Si}/\text{Al}_2\text{O}_3$ sample, measured with lock-in techniques, are in line with our previous work with height-voltage spectroscopy⁶ for the magnitude, lateral size, and correlation with the topography. The correlation between CPD and topography is probably a result of the ALD process, since the correlation is significantly stronger than for the thermal SiO_2 reference sample. However, the correlation cannot be used to visualize substrate inhibition since an equally strong correlation is observed for Al_2O_3 films deposited on a thin layer of thermal SiO_2 , whereas XPS measurements do not show evidence for substrate-inhibited growth on this starting surface. On the contrary, differential capacitance images show that

the cross correlation between topography and capacitance for ALD deposition on hydrogen-terminated Si is twice as high as for deposition on thermal oxide and five times higher than for thermal oxide only. This difference can be explained as follows: for ideally homogeneous, noninhibited growth the final height variations on the film (roughness) are expected to be a copy of the height variations of the starting surface. When the AFM tip scans the surface, it closely follows those height variations at a certain tip-sample separation and the capacitance between tip and substrate does not depend on the lateral position. In the case of surface-inhibited growth, the final height variations are dominated by nucleation of the ALD process, leading to a locally larger oxide thickness on the places where the nucleation initially took place. When the tip follows the surface topography, a higher topography will correspond to a larger local oxide thickness and hence a lower capacitance, exactly corresponding to the observed cross correlation. The observation that the topography-capacitance correlation for Al_2O_3 deposited on a substrate with thermal SiO_2 is higher than for the SiO_2 reference sample raises the question whether the growth on thermal oxide is fully noninhibited. Indeed it has been reported² that the growth on SiO_2 is not fully linear for deposited thicknesses below ~ 2.6 nm, which might explain the higher cross correlation with respect to bare SiO_2 .

We have shown that differential capacitance imaging, an extension to CPD measurements with KPFM, can visualize substrate-inhibited ALD growth. This technique shows a high potential for noninvasive investigation of the growth mode of thin films in an early stage of the growth.

¹G. D. Wilk, R. M. Wallace, and J. M. Anthony, *J. Appl. Phys.* **89**, 5243 (2001).

²L. G. Gosset, J.-F. Damlencourt, O. Renault, D. Rouchon, Ph. Holliger, A. Ermolieff, I. Trimaille, J.-J. Ganem, F. Martin, and M.-N. Séméria, *J. Non-Cryst. Solids* **303**, 17 (2002).

³M. Copel, M. Gribelyuk, and E. Gusev, *Appl. Phys. Lett.* **76**, 436 (2000).

⁴M. M. Frank, Y. J. Chabal, M. L. Green, A. Delabie, B. Brijs, G. D. Wilk, M.-Y. Ho, E. B. O. da Rosa, I. J. R. Baumvol, and F. C. Stedile, *Appl. Phys. Lett.* **83**, 740 (2003).

⁵R. Ludeke and E. Gusev, *J. Appl. Phys.* **96**, 2365 (2004).

⁶J. M. Sturm, A. I. Zinine, H. Wormeester, B. Poelsema, R. G. Bankras, J. Holleman, and J. Schmitz, *J. Appl. Phys.* **97**, 063709 (2005).

⁷S. Kitamura and M. Iwatsuki, *Appl. Phys. Lett.* **72**, 3154 (1998).

⁸Nanosensors™ CDT-FMR, www.nanosensors.com

⁹E. Hecht, *Optics*, 3rd ed. (Addison-Wesley, Reading, MA, 1998), p. 542.